Geomorphic response to uplift along the Dragon's Back pressure ridge, Carrizo Plain, California

George E. Hilley* Department of Geological and Environmental Sciences, Stanford University, Stanford, California 94305, USA
J Ramón Arrowsmith School of Earth and Space Exploration, Arizona State University, Tempe, Arizona 85287, USA

ABSTRACT

We used high-resolution topography, geomorphic mapping of active surface processes, and geologic mapping to study the topographic and erosional response of small drainage basins to rock uplift along the Dragon's Back pressure ridge along the San Andreas fault in the Carrizo Plain, California. We infer the history of deformation experienced by ~40 small drainage basins formed in poorly consolidated sedimentary rocks. A space-for-time substitution directly images the erosional and topographic responses to deformation. Progressive deformation and rock uplift are accompanied by increases in channel steepness and basin relief. As uplift ceases, channel concavity rapidly increases, causing channels to undercut hillslopes—this undercutting promotes the consumption of hillslopes by landsliding. This undercutting also causes basin relief to be greatest after uplift has stopped. This analysis indicates that channels of the Dragon's Back pressure ridge respond to changes in rock uplift rates over thousands of years, whereas hillslope processes may take more than an order of magnitude longer to adjust to changes in rock uplift rates. Our study directly measures changes in erosional processes due to the initiation and cessation of rock uplift, which can typically only be inferred using numerical models, by direct field observations.

Keywords: LiDAR data, landscape development, San Andreas fault, hillslope response, channel response.

INTRODUCTION

Reading tectonic deformation of Earth's surface from topography is a complicated endeavor because landscapes reflect both tectonic deformation and the ensuing response of surficial processes. These responses may be strongly coupled to one another and may vary depending on the rates of deformation, the climate (e.g., Knox, 1983; Tucker and Slingerland, 1997), and the physical and chemical properties of the underlying bedrock (e.g., Heimsath et al., 1997). Despite these complexities, much progress has been made in understanding how channel steepness in bedrock channels (e.g., Snyder et al., 2000; e.g., Whipple and Tucker, 1999), ridge-top to outlet elevations in analogue models (Lague et al., 2003), and mean elevation of catchments (e.g., Whipple and Meade, 2004; Willgoose et al., 1991) might vary with differing rock uplift rates. Much of what is known about how topography responds to changes in rock uplift rates has been gleaned from field studies that have attempted to relate topographic responses to a single, dominant erosional process, such as bedrock channel incision (e.g., Snyder et al., 2000; e.g., Whipple and Tucker, 1999). However, interactions between hillslope and channel processes may play an important role in controlling the topographic response to changes in rock uplift rates. These interactions may be difficult to study in the field because nature rarely provides us with sufficient information to acquire a detailed time series of the rock motions as well as the topographic and erosional response over the appropriate time scales (10^3–10^5 yr) (e.g., Fernandes and Dietrich, 1997; Roering et al., 2001; Whipple and Tucker, 1999) necessary to directly study such responses. For this reason, numerical models representing the effects of erosion through quasi–physically based transport laws (Dietrich et al., 2003) are instead used to infer the response of topography and erosion to deformation (Howard, 1994; Tucker and Bras, 1998; Tucker and Slingerland, 1997; van der Beek and Braun, 1998; Willgoose et al., 1991).

In this study, we report observations from the ~4.5-km-long Dragon's Back pressure ridge adjacent to the San Andreas fault in the Carrizo Plain of central California (Fig. 1). Here, fortuitous geologic circumstances allow us to construct a detailed time series of the motion of rocks comprising the pressure ridge, and the response of erosional processes and topography to changes in rock uplift rates. Detailed geologic field observations based on 1:8000-scale geologic mapping and aerial photograph interpretations constrain its deformation, geomorphic observations constrain processes eroding the landform, and recently acquired Airborne Laser Swath Mapping (ALSM) data provide high-resolution topographic data (1 m pixels) that characterize the topographic response. These data provide an excellent opportunity to examine how erosional processes change with the initiation and cessation of rock uplift, and how these changes are reflected in topographic metrics used to infer active rock uplift rates.

GEOLOGIC OBSERVATIONS

Geologic units within the Dragon's Back pressure ridge consist of the poorly consolidated, Pliocene-Pleistocene Paso Robles Formation (interbedded sandstone and conglomerates) (Arrowsmith, 1995). In the southeastern portion of the ridge, these units are flat lying, and only the uppermost Gold Member is exposed at the surface (Fig. 1B). Toward the northwest, progressively deeper portions of this sedimentary package have been exhumed (Tan and Pink Members) as the units have been folded and eroded. Both surface mapping and magnetotelluric cross sections (Unsworth et al., 1999) image structures inferred to accommodate San Andreas fault–normal contraction, and this contraction has apparently offset the San Andreas fault in the shallow subsurface beneath the southeastern end of the Dragon's Back pressure ridge. At >600 m depth, the San Andreas fault is offset toward the southwest relative to its surface trace (Fig. 1B). This step in the fault surface is linked to contraction accommodated by thrusting on the northeastern side of the San Andreas fault, and this fault step has localized deformation within the southeastern portion of the Dragon's Back pressure ridge. This geometric irregularity in the San Andreas fault appears to be anchored to the northeastern side (North American plate) of the fault. Thus, as right-lateral motion along the fault translates material of the Pacific plate northwestward into this obstruction along the fault surface, the initially flat-lying Paso Robles Formation is folded, uplifted, and faulted (see also Figure DR1 in the GSA Data Repository[1] for depiction of fault geometry). Once it passes the obstruction, deformation ceases. Because this structural knuckle has remained anchored to the North American plate for at least the last 130 k.y., the northwestern portions of the Dragon's Back pressure ridge can be viewed as having entered and left the knuckle in the relatively distant past, while those along its southeastern end are currently deforming. Importantly, the extent of warping of the geologic units bounds the topography of the pressure ridge, indicating that the topography has been formed and is controlled by deformation of the sur-

*E-mail: hilley@stanford.edu.

[1]GSA Data Repository item 2008092, additional structural information, photographic documentation of landscapes, and Airborne Laser Swath Mapping (ALSM) observations, is available online at www.geosociety.org/pubs/ft2008.htm, or on request from editing@geosociety.org or Documents Secretary, GSA, P.O. Box 9140, Boulder, CO 80301, USA.

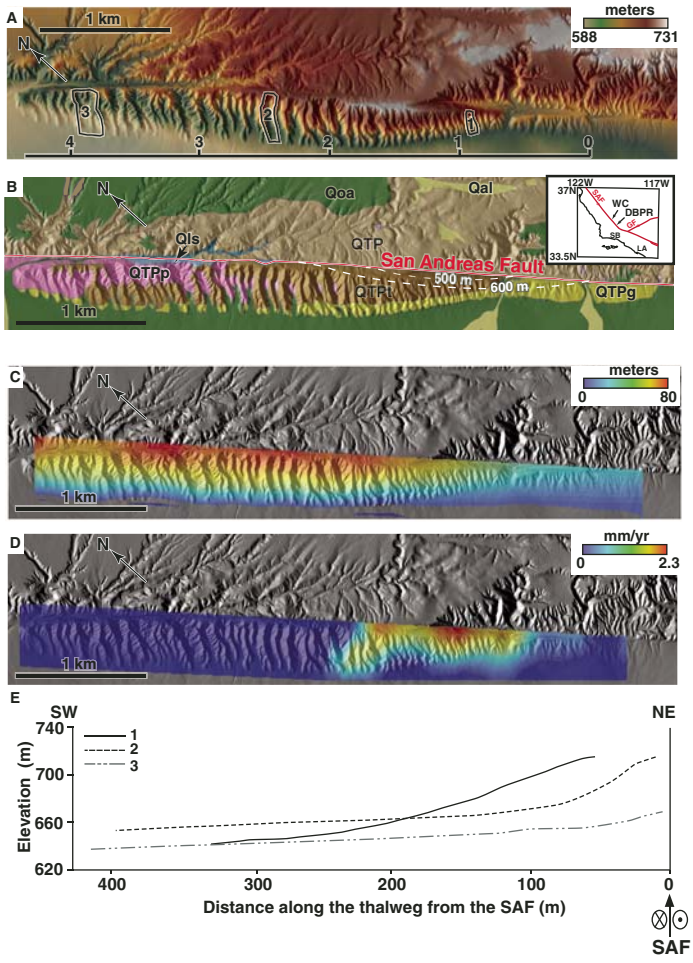

Figure 1. Dragon's Back pressure ridge (DBPR) and relatively stationary uplift zone. A: Airborne Laser Swath Mapping (ALSM) topography (1 m digital elevation model [DEM]); B: geology (modified from Arrowsmith, 1995); C: total rock uplift (sensu England and Molnar, 1990) inferred from distribution of geologic contacts, assuming initially horizontal contacts; D: instantaneous rock uplift rate (assuming 33 mm/yr of right-lateral slip along San Andreas fault [SAF]); and E: along-channel profiles of basin numbers referenced to panel A (see Figure DR2 for photographs of these basins [see text footnote 1]). In A, scale at bottom of panel references locations in Figure 2. In B, QTP is undifferentiated Paso Robles Formation; Qoa is Pleistocene alluvium; QTPp, QTPt, QPTg are pink, tan, and gold members of the Paso Robles Formation; Qls indicates landslide deposits; and Qya is young alluvium. Dashed contours in B show inferred location of San Andreas fault at various depths and illustrate shallow offset of San Andreas fault that produces rock uplift within southeastern portion of landform. Inset in B shows location of study area and highlights surrounding features: WC—Wallace Creek, GF—Garlock fault, SB—Santa Barbara, and LA—Los Angeles.

face, rather than by purely geomorphic processes. This allows us to make a space-for-time substitution in which the distance along the San Andreas fault to the northwest (relative to the beginning, or southeastern edge, of the structural knuckle) may be used with the long-term slip rate along the San Andreas fault to produce a time series of deformation experienced by each part of the landform. Studies at Wallace Creek, located in the northern Carrizo Plain, constrain the long-term (k.y.) strike-slip rate along the San Andreas fault in this area to between 32 and 35 mm/yr (Sieh and Jahns, 1984). Thus, each kilometer of length along the Dragon's Back pressure ridge (from southeast to northwest) represents ~33 k.y. of time since material of the Pacific plate entered the structural knuckle.

Geologic contacts between different members of the Paso Robles Formation define the deformation sustained within the Dragon's Back pressure ridge. We identified the elevation of these contacts using the ALSM data and our geologic mapping, and then we used their three-dimensional geometry to reconstruct folding within the landform (Fig. 1C) by interpolating and extrapolating their elevations to the edges of the Dragon's Back pressure ridge. Folding includes both vertical and fault-normal horizontal displacements—here, we show only the rock uplift (vertical component of displacement) for simplicity. However, bedding planes within the Dragon's Back pressure ridge dip ~30° on average within the fold hinge and show significant local variability (Arrowsmith, 1995). Thus, we expect the horizontal component of deformation to play an important, albeit lesser role than vertical deformation in determining attributes such as hillslope and channel steepness. Using the space-for-time substitution, the values of rock uplift can be used to estimate the spatial distribution of rock uplift rates within the Dragon's Back pressure ridge (Fig. 1D), and, taken together, these measurements provide our best estimate of the motion of each point within the Dragon's Back pressure ridge.

GEOMORPHIC AND TOPOGRAPHIC OBSERVATIONS

Channels, landslide scars, and basin boundaries were mapped on stereo aerial photography and in the field and were georeferenced to our ALSM digital elevation model (DEM). Channels were identified as those areas of the landscape that collect flow and show profile concavity, while debris-flow scars typically had more planar profiles. While it is likely that some channels that host debris flows have significant concavity, Stock and Dietrich (2003) noted that areas dominated by debris-flow incision typically display lower profile concavity than their downstream, fluvially dominated counterparts. Interestingly, while all basins had areas <1 km^2 (areas of the landscape we might expect debris-flow incision to be a dominant erosional process; Montgomery and Foufoula-Georgiou; 1993), there were nonetheless extensive portions of the channel network that displayed concavities (sensu Wobus et al., 2006) similar to channels in which fluvial transport typically dominates (Fig. 2). Along the southeastern end of the pressure ridge, basin areas and widths (measured parallel to the San Andreas fault) are small (Fig. 2). As the pressure ridge undergoes sustained deformation, basin areas increase as the width of the fold grows to the northwest and basins lengthen perpendicular to the fault (Figs. 1 and 2). As rock uplift ceases to the northwest, valleys widen, while basin lengths continue to track the edge of the deformed units in the Dragon's Back pressure ridge (Fig. 1). This valley widening lowers basin divides between adjacent basins and across the San Andreas fault; this promotes capture and amalgamation of adjacent basins to the northwest (Fig. 1).

Channel steepness has recently been proposed as a metric that faithfully records rock uplift rates in catchments where channels incise bedrock and rock uplift is balanced by erosion (Whipple and Tucker, 1999). Interestingly, while the Dragon's Back pressure ridge is underlain by unconsolidated material, and we might expect the small catchments here to be dominated by debris-flow incision and transport, channel steepness nonetheless increases directly with rock uplift (Fig. 2). High channel steepness is accompanied by modest increases in channel concavity. Even in this transient landscape where rock uplift and erosion are not in balance, as uplift rates cease, channel steepness rapidly decreases; however, channels become more concave toward the northwest edge of the uplift zone and reach a maximum concavity after uplift ceases (Fig. 2). This effect can also be seen in the profile concavity of surveyed channels of basins directly in the wake of the uplift zone (Figs. 1A and 1E, channel 2) relative to those before and after it (Figs. 1A and 1E, channels 1 and 3; see also supplementary Figures DR1 and DR2 for field- and ALSM-based observations of changing concavity [see footnote 1]). After this transient period of high concavity, channels become less concave (Fig. 2) as the headwater portions of the channels lower (Fig. 1E, channel 3). About 1.0–1.5 km from the

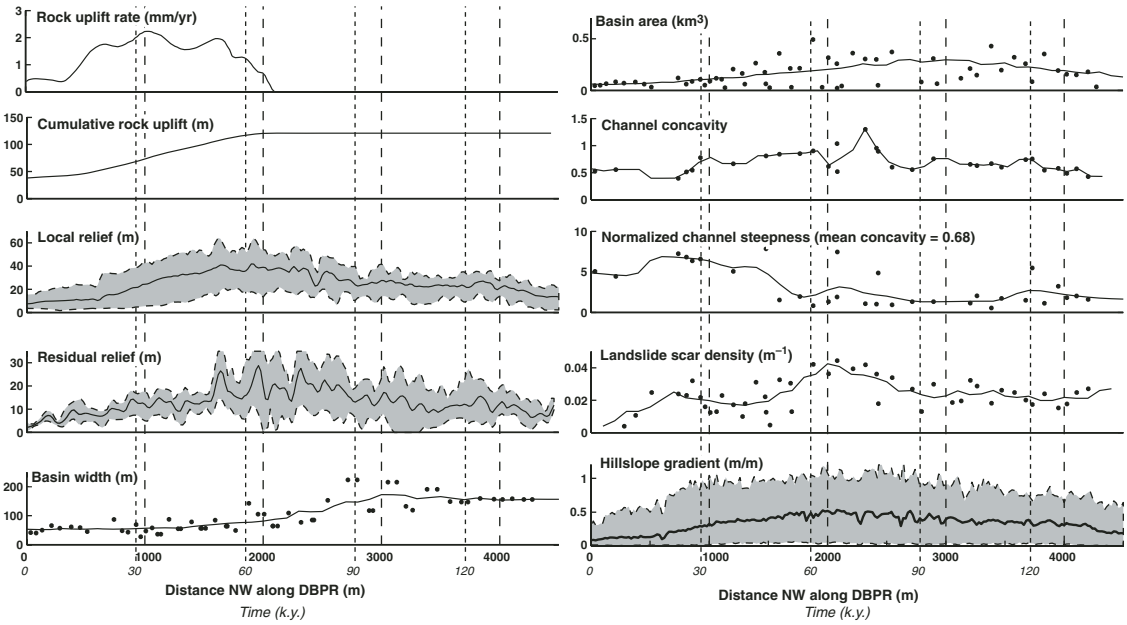

Figure 2. Mean rock uplift rates along DBPR ridge line, total rock uplift (measured peak values are from Fig. 1C), local relief (mean value shown as solid line, 95% bounds shown as shaded area), residual relief (mean value shown as solid line, 95% bounds shown as shaded area), basin width (solid line shows 500 m running average), basin area (solid line shows 500 m running average), channel concavity (solid line shows 200 m running average), normalized channel steepness (solid line shows 500 m running average), landslide scar density (solid line shows 500 m running average), and gradient along nonchannel points (mean value shown as solid line, 95% bounds shown as shaded area) shown as a function of distance from SE end of Dragon's Back pressure ridge (DBPR). Different averaging window for channel concavity was selected to highlight abrupt increase in concavity following cessation of uplift. Channel concavities and steepness (calculated using methods discussed in Whipple and Tucker, 1999) were calculated for those basins over which points that displayed a clear linear trend in log area–log slope space could be identified over more than one order of magnitude change in area. Normalized channel steepness was calculated by using mean concavity for all basins (0.68).

southeast edge of the pressure ridge, hillslopes become sufficiently steep to initiate shallow landslides and debris flows, and the mapped density of landslide scars (landslide scar length normalized to basin area) increases in this area as a result (Fig. 2). As with channel concavity, the density of landslide scars tends to be largest in the wake of the uplift zone; further to the northwest, landslide scar densities decrease (Fig. 2). In basins along the northwestern edge of the Dragon's Back pressure ridge, channel steepness is low, and channels maintain a constant concavity. It is here that landslide scar densities and channel steepness have declined in response to the cessation of rock uplift.

We used the ALSM 1 m DEM to calculate two landscape metrics that have been used in the past to infer tectonic activity from topography (e.g., Bullard and Lettis, 1993) to assess their performance in tracking rock uplift rates. We chose local relief (the range in elevation values contained within a circular search kernel) because of its widespread use in tectonic geomorphology studies, and residual relief (the difference between surfaces constructed from ridge-line and channel-bottom points) because of its previous use and intuitive appeal that basin relief likely changes with rock uplift rates. Both measures of relief increase along the southeastern third of the Dragon's Back pressure ridge located within the structural knuckle (Fig. 2). However, both also attain maximum values after points in the Dragon's Back pressure ridge move out of the zone of high rock uplift rates (Fig. 2). To the northwest of this relief maximum, both metrics decrease until only subtle relief is observed at the northwest end of the landform.

INTERPRETATION AND DISCUSSION

The space-for-time substitution used to infer rock uplift rates along the Dragon's Back pressure ridge can be equally well applied to the topographic and geomorphic development of the landform. In this way, we view each basin along the Dragon's Back pressure ridge as a different stage in the development of a single basin subject to a known deformation history. In addition, the unconsolidated sediments within the Dragon's Back pressure ridge have approximately uniform vegetation density, and contrasts between different units can only be identified by subtle contrasts in color on aerial photographs and bedding contacts in hand-dug excavations. Thus, our field experience suggests to us that it is improbable that the observed trends in channel and hillslope steepness have been largely influenced by contrasts in underlying substrate properties. This allows us to image the impact of rock uplift on topography without additional confounding factors. Our combined geologic, geomorphic, and topographic observations can thus be used to understand the relationships between, and adjustment time scales of, channel and hillslope processes as they respond to the initiation and cessation of rock uplift.

Using the mapped distribution of geomorphic processes and the ALSM topography, we see that relief gradually increases between 0 and 1 km from the southeast edge of the Dragon's Back pressure ridge (0–33 k.y. after the initiation of rock uplift), increases more rapidly until ~2 km (33–66 k.y.), and steadily decreases until 4.4 km (145 k.y.). Channel densities (channel length normalized to basin area) do not appear to vary in response to uplift, but channel steepness tends to faithfully track rock uplift rates (Fig. 2), as is predicted theoretically for fluvial channels that incise bedrock (Whipple and Tucker, 1999). By 2.1 km (66 k.y.), channel concavity becomes large and attains a maximum value by 2.3 km (76 k.y.), after which time, concavities rapidly return to pre-uplift values (Fig. 2). This change in channel concavity accompanies downcutting of the channels in response to the cessation of uplift. This process of downcutting, represented by decreasing channel steepness and changes in channel concavity, appears to occur between 2.1 km (the end of uplift) and 2.3 km, and so channels take ~6.6 k.y. to adjust to the cessation of uplift. Meanwhile, landslide scar densities increase within the uplift zone and apparently dominate the majority of hillslope transport after uplift has ceased (Fig. 2). This pattern results from rapid channel incision, which undercuts hillslopes, and the steepened hillslopes are then dominated by landsliding processes (e.g., Dietrich et al., 1992). The same increase in channel concavity that triggers landsliding also creates large amounts of ridge-to-channel relief in the basins as the rapidly downcutting channels deepen basins far below their ridgelines. This accelerated hillslope transport reduces hillslope gradients, and landslide scar densities decrease along the northwestern third

of the landform as mass-wasting processes eventually give way to more continuous diffusive transport, which produces smooth, upward-convex hillslopes (e.g., Black and Montgomery, 1991; Carson and Kirkby, 1972) (Fig. 2). This transition from mass-wasting to diffusive (likely bioturbative) transport occurs gradually until ~4 km (132 k.y.; ~73 k.y. after uplift has ceased), after which evidence of mass wasting is less common than within and directly adjacent to the zone of active rock uplift. Thus, the rapid response time of channels (~6.6 k.y.) relative to hillslopes (~73 k.y.) clearly affects the relief structure, as well as the spatial and temporal distribution of geomorphic processes acting to erode this landform.

We use direct field observations to quantify the differing responses of hillslope and channel processes and their impact on topography to changes in deformation over time scales that are likely appropriate for the formation of landform-scale topography. In relatively simple landscapes that are underlain by unconsolidated material (assumed analogous to well-studied soil-mantled landscapes), the topographic response to the initiation and cessation of rock uplift depends on the history of deformation rates and inter-relationships between the different erosional process responses to this history. Local and residual relief and the distribution of erosional processes generally track rock uplift rates, but more rapid channel response relative to hillslopes may produce significant lags between these topographic metrics and changes in rock uplift rates. In the case of the Dragon's Back pressure ridge, hillslope response times appear significantly longer than those of channels, which may be unexpected based on models of rapidly lowering landscapes (Whipple and Tucker, 1999). As channels undercut hillslopes sufficiently to initiate widespread mass wasting, the initiation of landsliding processes allows hillslopes to rapidly adjust, and it is the return to diffusive hillslope conditions that heralds longer response times, as might be expected from studies of these types of slopes (e.g., Fernandes and Dietrich, 1997; Roering et al., 2001). Interestingly, channel processes appear to respond most simply and rapidly to changes in rock uplift rates, even when basinwide elevations are increasing, and so, at least in the Dragon's Back pressure ridge, metrics such as channel steepness provide the most reliable measure of rock uplift rates.

ACKNOWLEDGMENTS

Funding for Hilley was provided by a National Aeronautics and Space Administration (NASA) Earth Systems Science Graduate Fellowship and U.S. Geological Survey (USGS) National Earthquake Hazards Reduction Program grant 1434-94-G-2464. Thanks are due to D. Rhodes for his help on the early development of these concepts. We thank J. Roering, W. Dietrich, M. Oskin, and C. Wobus for reviews of this manuscript. The National Center for Airborne Laser Mapping provided the Airborne Laser Swath Mapping (ALSM) data as a Seed Grant.

REFERENCES CITED

Arrowsmith, JR, 1995, Coupled Tectonic Deformation and Geomorphic Degradation along the San Andreas Fault Zone [Dissertation thesis]: Stanford, Stanford University, 346 p.

Black, T.A., and Montgomery, D.R., 1991, Sediment transport by burrowing animals, Marin County, California: Earth Surface Processes and Landforms, v. 16, p. 163–172, doi: 10.1002/esp.3290160207.

Bullard, T.F., and Lettis, W.R., 1993, Quaternary fold deformation associated with blind thrust faulting, Los Angeles Basin, California: Journal of Geophysical Research, v. 98, p. 8,349–8,369.

Carson, M.A., and Kirkby, M.J., 1972, Hillslope Form and Process: Cambridge, UK, Cambridge University Press, 475 p.

Dietrich, W.E., Wilson, C.J., Montgomery, D.R., McKean, J., and Bauer, R., 1992, Erosion thresholds and land surface morphology: Geology, v. 20, p. 675–679, doi: 10.1130/0091–7613(1992)020<0675:ETALSM>2.3.CO;2.

Dietrich, W.E., Bellugi, D.G., Sklar, L.S., Stock, J.D., Heimsath, A.M., and Roering, J.J., 2003, Geomorphic transport laws for predicting landscape form and dynamics, *in* Wilcock, P.R., and Iverson, R.M., eds., Prediction in Geomorphology: American Geophysical Union Geophysical Monograph 135, p. 103–132.

England, P.C., and Molnar, P., 1990, Surface uplift, uplift of rocks, and exhumation of rocks: Geology, v. 18, p. 1173–1177, doi: 10.1130/0091–7613(1990)018<1173:SUUORA>2.3.CO;2.

Fernandes, N.F., and Dietrich, W.E., 1997, Hillslope evolution by diffusive processes; the timescale for equilibrium adjustments: Water Resources Research, v. 33, p. 1307–1318, doi: 10.1029/97WR00534.

Heimsath, A.M., Dietrich, W.E., Nishiizumi, K., and Finkel, R.C., 1997, The soil production function and landscape equilibrium: Nature, v. 388, p. 358–361, doi: 10.1038/41056.

Howard, A.D., 1994, A detachment-limited model of drainage basin evolution: Water Resources Research, v. 30, p. 2261–2285, doi: 10.1029/94WR00757.

Knox, J.C., 1983, Responses of river systems to Holocene climates, *in* Wright, H.E., Jr., ed., Late-Quaternary Environments of the United States, Volume 2: Minneapolis, University of Minnesota Press, p. 26–41.

Lague, D., Crave, A., and Davy, P., 2003, Laboratory experiments simulating the geomorphic response to tectonic uplift: Journal of Geophysical Research, v. 108, doi: 10.1029/2002JB001785, 2003.

Montgomery, D.R., and Foufoula-Georgiou, E., 1993, Channel network representation using digital elevation models: Water Resources Research, v. 29, p. 3925–3934, doi: 10.1029/93WR02463.

Roering, J.J., Kirchner, J.W., and Dietrich, W.E., 2001, Hillslope evolution by nonlinear, slope-dependent transport: Steady state morphology and equilibrium adjustment timescales: Journal of Geophysical Research, ser. B, Solid Earth and Planets, v. 106, p. 16,499–16,513, doi: 10.1029/2001JB000323.

Sieh, K.E., and Jahns, R.H., 1984, Holocene activity of the San Andreas fault at Wallace Creek, California: Geological Society of America Bulletin, v. 95, p. 883–896, doi: 10.1130/0016–7606(1984)95<883:HAOTSA>2.0.CO;2.

Snyder, N.P., Whipple, K.X, Tucker, G.E., and Merritts, D.J., 2000, Landscape response to tectonic forcing: Digital elevation model analysis of stream profiles in the Mendocino triple junction region, northern California: Geological Society of America Bulletin, v. 112, p. 1250–1263, doi: 10.1130/0016–7606(2000)112<1250:LRTTFD>2.3.CO;2.

Stock, J.D., and Dietrich, W.E., 2003, Valley incision by debris flows: Evidence of a topographic signature: Water Resources Research, v. 39, p. 1089, doi: 10.1029/2001WR001057.

Tucker, G.E., and Bras, R.L., 1998, Hillslope processes, drainage density, and landscape morphology: Water Resources Research, v. 34, p. 2751–2764, doi: 10.1029/98WR01474.

Tucker, G.E., and Slingerland, R., 1997, Drainage basin response to climate change: Water Resources Research, v. 33, p. 2031–2047, doi: 10.1029/97WR00409.

Unsworth, M., Egbert, G., and Booker, J.R., 1999, High-resolution electromagnetic imaging of the San Andreas fault in central California: Journal of Geophysical Research, ser. B, Solid Earth and Planets, v. 104, p. 1131–1150.

van der Beek, P., and Braun, J., 1998, Numerical modelling of landscape evolution on geological time-scales: A parameter analysis and comparison with the southeastern highlands of Australia: Basin Research, v. 10, p. 49–68, doi: 10.1046/j.1365–2117.1998.00056.x.

Whipple, K.X, and Meade, B.J., 2004, Controls on the strength of coupling among climate, erosion, and deformation in two-sided, frictional orogenic wedges at steady-state: Journal of Geophysical Research–Earth Surface, v. 109, p. F01011, doi: 10.1029/2003JF000019.

Whipple, K.X, and Tucker, G.E., 1999, Dynamics of the stream-power river incision model: Implications for height limits of mountain ranges, landscape response timescales, and research needs: Journal of Geophysical Research, ser. B, Solid Earth and Planets, v. 104, p. 17,661–17,674, doi: 10.1029/1999JB900120.

Willgoose, G., Bras, R.L., and Rodriguez-Iturbe, I., 1991, A coupled channel network growth and hillslope evolution model. 1: Theory: Water Resources Research, v. 27, p. 1671–1684, doi: 10.1029/91WR00935.

Wobus, C., Whipple, K.X, Kirby, E., Snyder, N.P., Johnson, J., Spyropoulou, K., Crosby, B., and Sheehan, D., 2006, Tectonics from topography: Procedures, promise, and pitfalls, *in* Willett, S.D., et al., eds., Tectonics, Climate, and Evolution: Geological Society of America Special Paper 298, Penrose Conference Series, p. 55–74, doi: 10.1130/2006.2398(04).

Manuscript received 29 October 2007
Revised manuscript received 4 January 2008
Manuscript accepted 19 January 2008

Printed in USA